Elastic Properties of Viruses

B. Stephanidis,* S. Adichtchev,* P. Gouet,† A. McPherson,‡ and A. Mermet*
*Laboratoire de Physico-Chimie des Matériaux Luminescents, Université Lyon 1, Villeurbanne, France; †Institut de Biologie et Chimie des Protéines, Université Lyon 1, Lyon, France; and ‡Department of Molecular Biology and Biochemistry, University of California, Irvine, California USA

ABSTRACT Viruses are compact biological nanoparticles whose elastic and dynamical properties are hardly known. Inelastic (Brillouin) light scattering was used to characterize these properties, from microcrystals of the Satellite Tobacco Mosaic Virus, a nearly spherical plant virus of 17-nm diameter. Longitudinal sound velocities in wet and dry Satellite Tobacco Mosaic Virus crystals were determined and compared to that of the well-known protein crystal, lysozyme. Localized vibrational modes of the viral particles (i.e., particle modes) were sought in the relevant frequency ranges, as derived assuming the viruses as full free nanospheres. Despite very favorable conditions, regarding virus concentration and expected low damping in dry microcrystals, no firm evidence of virus particle modes could be detected.

INTRODUCTION

Viruses are biological objects with nanometric dimensions (typically from 10 nm to 100 nm) whose dynamical properties are poorly documented in contrast to their structural characterization allowed by x-ray crystallography and cryo-electron microscopy. As pointed out by Witz and Brown (1), the sole knowledge of virus structures may not be sufficient to account for alterations that occur upon interaction of the virus with its environment. For instance, it is well known that under specific conditions viruses undergo significant morphology changes (like swelling (1,2)) associated with transient local modifications of the virus structure; these changes inherently depend on the elastic properties of the virions that only very few experimental studies have reported on so far.

One important challenge in characterizing the dynamical properties of viruses is to assess the existence of collective vibrational modes that induce large-scale periodic deformations of the particle overall shapes. These types of modes (also referred to as particle modes) have long been studied for solid nanoparticles like metallic clusters or carbon nanotubes, allowing a unique characterization of the global elastic properties of the nano-objects. As mechanically tough, compact, and highly symmetrical particles, viruses have been predicted to possess similar modes of vibration, involving the coherent motions of their main constituents (3–8). Although not yet experimentally identified, recent normal mode analyses (NMA) performed on several viral capsids (9,10) suggested that such types of modes may be involved in some large scale structural rearrangements of viruses, thereby calling for further identifications of viruses' vibrational properties. Such modes were also evidenced through molecular dynamics simulations of a rhinovirus capsid (11).

In this article, we report an investigation on the dynamical properties of viruses through inelastic Brillouin light-scattering, providing a first determination of viruses' elastic parameters. These data are key information for the computation of vibrational mode frequencies (like NMA); they may also be useful in predicting the mechanical stability of viral structures (12,13). The sound velocity deduced from these measurements turns out to significantly differ from that of the archetype protein crystal, i.e., lysozyme, often used as reference data for normal mode calculations of viruses. During this study, we show that particle modes of viruses are not observed through inelastic light scattering, from either concentrated aqueous solutions or crystalline assemblies.

The virus under study is the Satellite Tobacco Mosaic Virus (STMV), for which extensive structural data exist (14,15). In addition, a very recent all-atom molecular dynamics simulation of the STMV gave unprecedented insights into the dynamical behavior of the complete virion (16). In the frame of our research, the choice for this virus is manifold. Firstly, as described further, the small size of this virus (~17 nm diameter) is associated with vibration mode frequencies ν that are sufficiently large ($\nu \geq \sim 5$ GHz) to be experimentally reached unambiguously. Secondly, the nearly spherical shape of the STMV (of actual icosahedral structure) makes it an ideal reference case for calculations based on the assumption of spherical particles (4,5,8). Another important aspect of STMV is that it is by far the easiest virus to produce in the form of microcrystallites that, in one respect, one can consider as the most concentrated virus samples.

SAMPLES AND EXPERIMENTAL METHODS

STMV samples

Different STMV samples associated with different conditionings were investigated: solutions, fully hydrated crystals (wet crystals) and severely dehydrated crystals (dry crystals).

Submitted March 19, 2007, and accepted for publication April 23, 2007.

Address reprint requests to A. Mermet, Tel.: 33-4-72-43-29-72; E-mail: mermet@pcml.univ-lyon1.fr.

S. Adichtchev is on leave from the IA&E Russian Academy of Sciences, Novosibirsk, 630090, Russia.

Editor: Jill Trewhella.

0006-3495/07/08/1354/06 $2.00

doi: 10.1529/biophysj.107.109033

The solution is a purified preparation of STMV that was twice recrystallized from NaCl, with a final concentration of 8.5 mg/ml (optical density of 1.8). The buffer solution is 0.025 M sodium sulfate at pH 6.8.

STMV crystals were grown using the hanging-drop method at room temperature. Crystals with sizes as large as 200 μm were obtained and transferred into sealed glass capillaries for x-ray diffraction (XRD) and for selected light-scattering experiments. Upon transfer, a minimum amount of surrounding mother liquor was kept to ensure full hydration and stability of the microcrystals. XRD patterns with 2 Å resolution assessed the good quality of the microcrystals, before and after the light-scattering experiments. All crystals investigated had orthorhombic unit cells.

The dry crystals were produced by slow evaporation of the mother liquor in unsealed capillaries over several days in air. Upon drying, the microcrystals become slightly opaque, losing their high resolution diffracting properties. However, an AFM characterization (Fig. 1) of a dry crystal kept over three months in air at room temperature shows that the STMV particles retain their globular shapes and the crystalline organization remains. The average size determined from the peak-to-peak height profile along several one-dimensional arrays visible in the picture is in good agreement with that determined from AFM measurements on wet microcrystals (17) (i.e., 17 nm).

Light-scattering experiments

The inelastic light-scattering experiments were achieved using a six-pass Sandercock tandem Fabry-Perot interferometer (18). Typically, this device is used to measure light inelastically scattered from acoustic sound excitations (Brillouin scattering) at very low frequencies ($\sim 1 \leq \nu \leq 30$ GHz). Recently, it has proved very successful in the characterization of particle modes from glass nanospheres embedded in colloidal assemblies (19–21).

The laser excitation used is the 532-nm line of a doubled Nd-YAG continuous laser. Experiments were performed in polarized and depolarized conditions, using a grid polarizer for the scattered radiation and the vertical polarization of the incident laser light. For all samples investigated, the laser power at the sample was set to 10 mW, inducing no damage of the samples as checked by XRD and assessed by the reproducibility of the measurements. Different scattering geometries (backscattering, 90A and 90R), described in details elsewhere (22), were used. The STMV solutions were investigated in backscattering geometry using fused quartz parallelepipedic cells. The microcrystals were studied either in capillaries (backscattering measurements) or in between sealed flat glass slides (90° measurements). For large spectral ranges (see last section), the STMV microcrystal was glued on a metal pin to avoid the Brillouin signal from the glass capillary. The precise crystallographic orientation of the microcrystals with respect to the transferred light wavevector Q could not be arranged in our light-scattering experiments. However, published Brillouin data on a lysozyme crystal (22) revealed that anisotropy effects (i.e., different sound velocities along different crystallographic orientations) amounted at most to 10% relative changes so that one can neglect them in a first approximation.

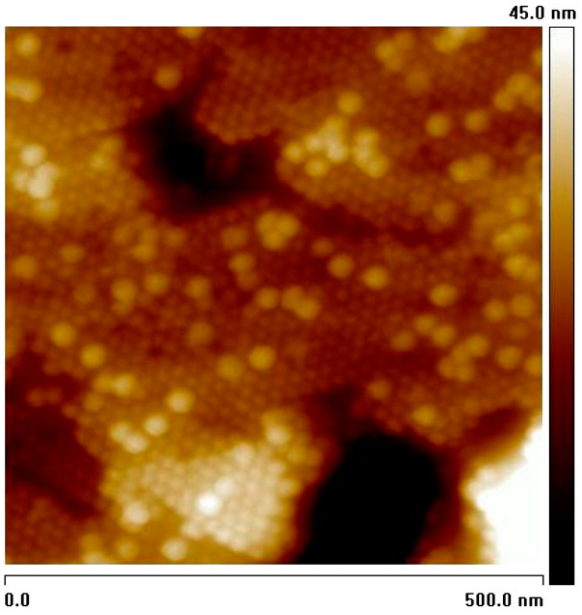

FIGURE 1 AFM picture from the surface of a dry STMV microcrystal. The size of the STMV particles determined from the peak-to-peak height profile is ~17 nm. Larger globules, possibly corresponding to aggregates of several virions, are also observed. The AFM measurements were made in tapping mode, at the frequency of 290 kHz, using a 15-nm silicon tip.

Brillouin scattering results

In the first place, STMV solutions were investigated. All corresponding spectra showed no other Brillouin signal than that of the aqueous buffer, probably because of too low STMV concentrations ($\sim 10^{-3}$% in volume). For this reason, subsequent studies focus on STMV crystals.

Fig. 2 displays the Brillouin spectrum of a wet STMV microcrystal, in backscattering geometry. While the narrow line at $\nu = 8 \pm 0.05$ GHz accounts for the neighboring aqueous buffer, the broader line at $\nu = 11.2 \pm 0.2$ GHz arises from the STMV crystal (the error figures are standard deviations obtained from measurements performed from different crystals). The full widths at half-maximum Γ derived from Lorentzian fits of the Brillouin lines are, respectively, 1.33 ± 0.07 GHz and 2.69 ± 0.06 GHz (no deconvolution was used since the observed linewidths are ~2 orders-of-magnitude larger than the instrumental resolution). Both of these lines correspond to longitudinal acoustic modes propagating in the respective media, as confirmed by their strong polarization and dependence upon scattering geometry. One can estimate the longitudinal sound velocity v_l in the STMV crystal from the value of the frequency ν using the backscattering geometry relation

$$\nu = \frac{2v_l n}{\lambda}, \tag{1}$$

where n is the refractive index of the scattering medium and λ the excitation wavelength. The evaluation of the refractive index can be obtained by

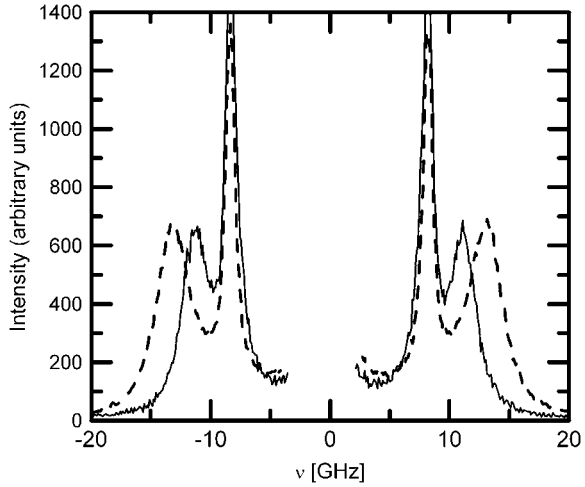

FIGURE 2 Polarized Brillouin spectrum of a wet STMV crystal in backscattering geometry (*solid line*). The Brillouin spectrum of a wet lysozyme crystal is shown for comparison (*dashed line*). The sharp lines at ±8 GHz arise from the surrounding aqueous buffer.

comparing the frequency shift of the Brillouin line upon changing the scattering geometry from backscattering to 90A or 90R. The so-deduced value of n is 1.55 ± 0.03, in agreement with that of protein matter crystals (22). It comes out that the longitudinal sound velocity in STMV crystals is 1920 ± 70 m/s. This value somewhat differs from that deduced from ultrasound measurements on a lysozyme crystal (1817 m/s (23)), which has often been used as reference data for calculations on viruses in the absence of virus elastic data. More recent Brillouin measurements on a lysozyme crystal (22) yielded a sound velocity of 2200 m/s (average over the (110) and the (001) directions), i.e., a value 20% larger than that deduced from ultrasound measurements for nearly identical hydration rates. Such discrepancy was ascribed to a frequency dependence of the sound velocity (22). Typically, the use of Brillouin determined values of the sound velocity is preferred over those determined from ultrasound measurements as light-scattering experiments probe matter over shorter wavelengths.

To clarify the difference between the elastic response of a lysozyme crystal and that of the STMV crystal, we have measured the Brillouin spectrum of a lysozyme crystal in the very same conditions as those used for the STMV measurements (immersed in the buffer solution, in backscattering geometry). The lysozyme crystals were grown according to the same method as that previously described for STMV crystals. Fig. 2 shows that the Brillouin line position of the wet lysozyme crystal (13 ± 0.6 GHz) is larger than that of the STMV crystal by ~15%, thereby confirming the difference between the protein crystal and the virus crystal. The sound velocity deduced from this position is 2230 m/s (with an identical refractive index of n = 1.55), in excellent agreement with the previous Brillouin measurements of Speziale et al. (22). It comes out from this comparison that a more thorough evaluation of mechanical properties of viruses will be obtained considering the actual elastic parameters of a virus crystal rather than those of a lysozyme crystal, at variance with assumptions made so far (6–8). In fact, the lower speed of sound in the virus crystal as compared to that in the lysozyme crystal may be related to a denser packing inside both the proteic capsid and the nucleotide core.

Further characterization of the acoustic phonon propagation in the STMV crystal can be given by the normalized sound attenuation parameter (24) (Λ), defined as the ratio of the Brillouin linewidth (Γ) with respect to its frequency position ν ($\Lambda = \pi\Gamma/\nu$). The normalized sound attenuation of Λ = 0.76 in the STMV crystal is close to that found for the wet lysozyme crystal (22), confirming that the sound attenuation process in wet organic crystals is essentially dominated by the hydration water of the biomolecules building up the crystals, quite irrelevantly to the nature of the biomolecules.

Upon drying, the Brillouin line shifts to ν = 20 ± 0.5 GHz (Fig. 3), leading to a speed of sound of v_l = 3430 ± 80 m/s, in fair agreement with trends reported for dehydrated lysozyme crystals (22). For dry crystals, the broadening of the Brillouin line is essentially controlled by the crystalline quality of the crystal over a few hundreds of nanometers, as experimentally verified with different samples. The typical sound attenuation values found for dry crystals ranged between that of the wet crystals (case shown in Fig. 3) and values as low as 0.3.

From the derived values of the sound velocity, one can give an estimate of the corresponding Young moduli E assuming that the anisotropy of the crystalline structure is weak and that the Poisson ratio σ of viruses is close to that of soft condensed matter, i.e., $\sigma \approx 0.3$ (25,26). Considering a mass density ρ of the wet STMV crystal close to that of wet lysozyme crystals (ρ = 1.2 g per cm^{-3}), one obtains $E \simeq 3.3$ GPa. This value, in fair agreement with more direct scanning force microscopy measurements on bacteriophage caspids (25), reflects the remarkable toughness of protein shells. Upon drying, the Young modulus estimate increases to ~10 GPa. The large Young moduli of dry virus assemblies make them unique organic nanotemplates for the fabrication of metallic or semiconductor nano-objects (27–29).

Finally, note that the transverse sound velocity in the STMV crystals could not be determined from the Brillouin spectra since no transverse excitation were observed. The lack of information concerning the transverse dynamics casts important uncertainties in the evaluation of viruses' particle mode frequencies, as explained in the next section.

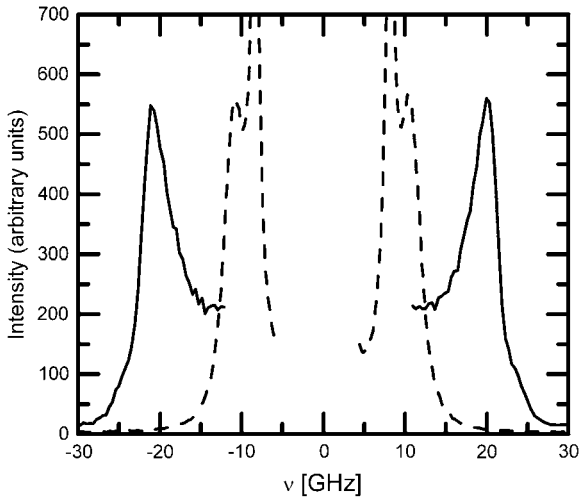

FIGURE 3 Polarized Brillouin spectrum of an air-dried STMV crystal in backscattering geometry (*solid line*). For comparison, the Brillouin spectrum of the wet crystal (Fig. 2) is also shown (*dashed line*).

Particle vibration modes in viruses

The study of particle modes in nanometric structures received great impetus with the growing emergence of nano-objects (nanosphere, nanorods, nanoprisms...). These types of modes were first detected in spherical nanocrystallites embedded in a glass, through inelastic Raman light scattering (30). Over the last two decades, this technique enabled the detection of low-frequency vibrational modes of a wide variety of nanoparticles, ranging from small (diameter D < 10 nm) metallic clusters to large (D ~ 100 nm) colloidal spheres (19–21). It has proved to be a powerful tool for evaluating the sizes of nanoparticles in a nondestructive way, but also, as a vibrational spectroscopy, it gives information on the interaction of the particle with its environment.

The existence of low frequency modes in rigid biological structures, together with their possible detection through inelastic light scattering, was first examined by de Gennes and Papoular (3). More recently, several theoretical and computational approaches focused on the cases of rod-shaped (6,7) and spherical-like (for icosahedral) (4,5,8) virus particles. The low frequency modes derived from these approaches, all based on the elastic continuous medium assumption, can be classified into two categories, radial and shear oscillations. In the case of a free nanosphere, the mode frequency ν is inversely proportional to the particle diameter D through the simplified relation

$$\nu = \frac{Sv}{D}, \tag{2}$$

where S is a shape factor (~0.8–0.9 for spherical objects) and v is the sound velocity in the nanosphere. The exact values of S and v to be entered in this relation differ according to the type of mode described by the nanosphere. The extensive description of these modes lies beyond the scope of this article. We will only consider here two modes in particular, namely the spherical mode (ν_0) and the quadrupolar mode (ν_2). The first one involves a radial breathing motion of the particle. It was suggested through NMA (10) that this mode is strongly involved in swelling transitions of several viral capsids. In the quadrupolar mode, the nanosphere deforms into transient oblate and prolate shapes over consecutive half periods of vibration. These two modes have proved to be the most easily detected ones through inelastic light scattering from many hard-condensed matter nanoparticles, in agreement with light-scattering selection rules (31); that is why we consider them as those to be most likely detected in the yet unexplored case of virus particles. Note that while ν_0 is proportional to the longitudinal sound

velocity ($\nu_0 = Sv_l/D$), ν_2 is proportional to the transverse sound velocity ($\nu_2 = Sv_t/D$) within the nanoparticle. Along their respective longitudinal and transverse characters, the spherical mode is expected to be polarized while the quadrupolar mode is expected to be depolarized, as experimentally observed for hard-condensed matter nanoparticles (32).

Equation 2 can be used for a rough estimation of ν_0 and ν_2, assuming viruses as full free nanospheres (4,5). In the following, we apply Eq. 2 to the case of STMV particles. Although such calculations rely on several assumptions, in particular with respect to the poorly known values of the virus acoustic parameters, they yield rather good estimates of the spectral ranges to be explored.

In a first approximation, we assume the STMV particles as full free nanospheres of 17-nm diameter. Taking into account the multilayerlike structure of the virion, such as that depicted by Freddolino et al. (16), is unnecessary for our exploration purposes since it is not expected to induce significant changes of the frequency values. An important ingredient of Eq. 2 is the value of the sound velocity within the vibrating particle. Applications of Eq. 2 with sound velocities determined through Brillouin light scattering have proved successful (30), so that one can take as longitudinal sound velocity $v_l = 1920$ m/s for a fully hydrated virus (wet crystal) and $v_l = 3350$ m/s for a totally dehydrated virus (dry crystal). The value of the transverse sound velocity (which is essential in the evaluation of ν_2) is much more of an issue, since the light-scattering experiments do not allow measuring it. Typical values of the ratio v_l/v_t range between 2 and 2.5 for condensed matter. To provide a range of possible values for ν_2, we have used as extreme cases $v_t = v_l/2$ and $v_t = v_l/4$ (very soft bodies (3)). Finally, the shape parameter S is set to 0.85, as a mean value for spherical objects. The slight dependence of S on the ratio v_l/v_t is negligible with respect to the uncertainty arising from the unknown transverse sound velocity (33).

From the above considerations, one obtains $\nu_0 \approx 96$ GHz and $\nu_2 \approx$ (24–48) GHz for a fully hydrated STMV particle. Exploration of these frequency ranges were performed by recording different spectra with different mirror spacings of the Fabry-Perot interferometer, thus allowing coverage of a total frequency range extending from a few GHz to ~100 GHz. Fig. 4 *a* shows the polarized and the depolarized large frequency range spectra of the wet STMV crystal. These spectra display the intense lines of Fig. 2 and, in addition, a sharp peak at ~30 GHz, corresponding to the Brillouin signal of the crystal container (silica capillary). Apart from these identified lines, no obvious additional inelastic feature is observed in either of the frequency ranges near ν_0 and ν_2. Note that this observation holds for the depolarized spectra where the ν_2 frequency region is cleared out of the strongly polarized capillary Brillouin line (at ~30 GHz).

As pointed out by Saviot et al. (5), the particle modes of viruses are expected to be severely damped when the viruses are embedded in a liquid. This is due to a near matching of the acoustic parameters of the virus itself and those of the liquid, leading to a strong broadening and softening of the inelastic excitation. The case of viruses immersed in water has recently been illustrated by Talati et al. (8) using the complex frequency model developed by Murray and Saviot (34,35). According to this study, water appears as a very unfavorable embedding medium for the observation of virus particle modes because of a weak acoustic impedance mismatch. In this latter respect, dry STMV crystals appear more favorable samples as most of the mobile water (26), which is likely to account for the damping of the modes, is removed. Taking into account the longitudinal sound velocity of 3430 m/s of the dry crystal, and on the basis of identical assumptions for v_t, one gets $\nu_0 \approx 171$ GHz while $\nu_2 \approx$ (43–86) GHz. Fig. 4 *b* shows the polarized and depolarized large frequency range spectra of the dry STMV crystal. Despite the favorable acoustic-impedance mismatch conditions, no significant inelastic feature is seen in these spectra. In a way, this conclusion meets the results of simulation works (16) on the STMV showing no coherent motion (in particular radial motion) of the STMV capsid. Nevertheless, one has to mention that some slight differences between the wet crystal (Fig. 4 *a*) and the dry crystal (Fig. 4 *b*) may be observed, apart from the shift of the Brillouin line upon drying: 1), the appearance of a weak bump at ~24 GHz in the dry crystal and 2), a very broad (nearly flat) signal below 10 GHz.

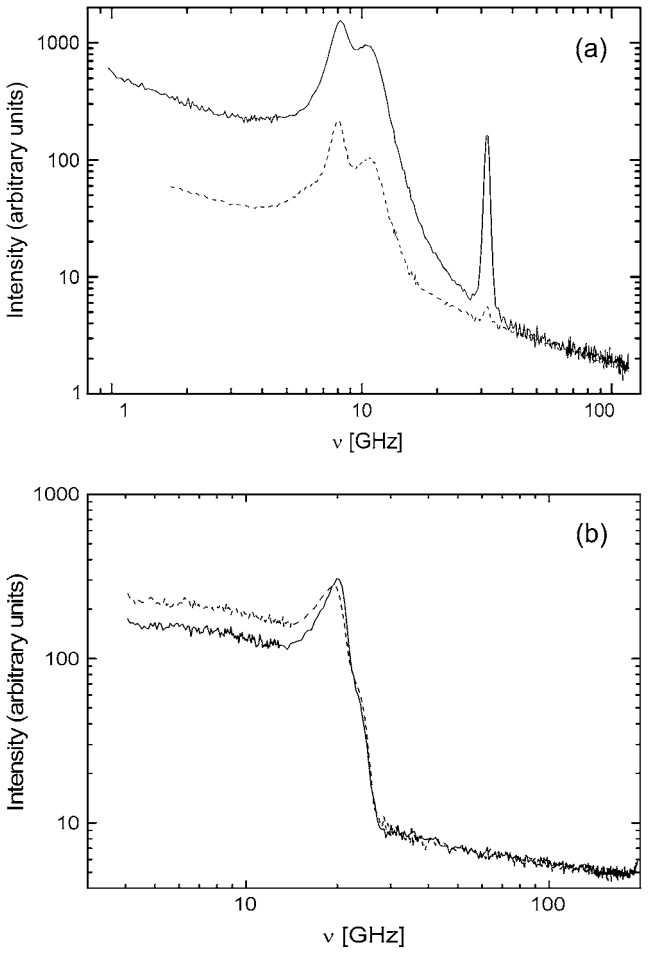

FIGURE 4 Large frequency range spectra (*solid lines*, polarized; *dashed lines*, depolarized) of (*a*) a wet STMV crystal and (*b*) a dry STMV crystal. For clarity, only the Stokes side of the spectra are shown. The sharp peak at ~30 GHz arises from the glass capillary.

While the bump at ~24 GHz may be associated with a possible trace of the quadrupolar particle mode (whose frequency would be much lower than that expected because of weaker local elastic constants), the broad signal below 10 GHz may be associated to the bound water confined in the core of the virus. Because it is weak and not resolved from the intense Brillouin line, the identification of the 24 GHz bump is extremely difficult. At the present stage, it can definitely not be considered as an evidence of a STMV particle mode.

Several explanations can be found for the nonobservation of particle modes from STMV viruses, in contrast with measurements from hard-condensed matter nanoparticles like metallic clusters (36,32), glass, or polymeric nanospheres (19–21). The first possible explanation is related to the virus structure itself. Despite the good mechanical global cohesion of the virus particles, as evidenced by AFM measurements, the cohesion between the virus constituents may not be stiff enough for coherent motions to settle throughout the composite structure. This can arise from the rather weak nondirectional interactions between the capsomers (in comparison with covalent bonds in hard-condensed matter nanoparticles) or within the viral proteins; it may also be related to insufficient symmetry of the virus core (16). Such arguments may also hold for the nonobservation of low frequency modes from globular proteins (37). In the case of viruses, these arguments conflict with results of NMA (9,10) that have identified normal modes of

several viral capsids, although it is worth mentioning that these works do not take into account the nucleotide core.

Another possibility is that the remaining bound water in STMV dry crystals, which is not so relevant in the propagation of acoustic modes whose wavelengths are large compared to the sizes of the viruses, is still the cause of strong damping of the particle modes. This is, however, rather unexpected if one considers the significant effect of drying on the low-frequency vibration modes of globular proteins (38). If particle modes that radiate acoustic power, like the breathing mode and the quadrupolar mode considered above, are strongly subject to damping by neighboring solvent molecules, it is less the case for torsional modes (3) whose frequencies lie in a comparable range, as that explored in the present study. Unfortunately, these modes are known to be inactive for the scattering of light (31) in the case of small objects like the STMV ($D \ll \lambda$).

Finally, the difficulty of detecting particle modes from viruses through inelastic light scattering may come from the limits of the technique itself. As a Raman process, inelastic scattering of light from particle modes occurs if these modes induce significant polarizability changes. It may be that for biological globules, these changes are too small to produce inelastic scattering. In these conditions, scattering enhancement methods like metallic nanoparticle labeling appear as promising alternatives. Another way of circumventing this difficulty is to adapt the light scattering probe to the size of the virus. Indeed, resonant scattering effects when $\lambda \sim D$ have proved very successful in the case of glass nanospheres (19–21). Particle modes from viruses with sizes of ~100 nm may then be detected using UV radiation as excitation wavelength.

CONCLUSION

In this article, we have reported Brillouin light-scattering experiments from a well-known plant virus, the Satellite Tobacco Mosaic Virus. The investigation of microcrystals of STMV led to the determination of the speed of sound in both wet and dry crystals. In full hydration conditions (wet crystals), the sound velocity value was found to significantly differ from that of a lysozyme crystal whose acoustic parameters have often been used to model mechanical properties of viral capsids. This difference underlines the need to take into account the specificities of viruses in modeling their elastic behavior. Upon air-drying, the STMV crystals considerably stiffen as indicated by an increase of sound velocity of ~80%, while the virions remain intact. This assesses the robustness of ordered virus arrays, a decisive feature for their use as nanotemplates.

Using the Brillouin light-scattering setup, we have explored the existence of vibrational modes that induce large-scale deformations of the viral particles (like the breathing motion). None of these modes could be clearly detected over a frequency range that largely encompasses that deduced from predicting calculations. Such observation holds for STMV in aqueous environment (solution and wet crystals) where severe damping of the modes is expected, as well as in dry crystals where acoustic impedance mismatch a priori favors their detection. We have proposed several explanations for the nonobservation of these modes; possible alternatives are currently under investigation.

The authors acknowledge A. Descamps for the AFM measurements and L. Saviot for discussions.

We thank Région Rhône-Alpes for partially funding this research.

REFERENCES

1. Witz, J., and F. Brown. 2001. Structural dynamics, an intrinsic property of viral capsids. *Arch. Virol.* V146:2263–2274.
2. Casselyn, M., J. Perez, A. Tardieu, P. Vachette, J. Witz, and H. Delacroix. 2001. Spherical plant viruses: interactions in solution, phase diagrams and crystallization of brome mosaic virus. *Acta Crystallograph. D.* 57:1799–1812.
3. De Gennes, P.-G., and M. Papoular. 1969. Low-frequency vibrational modes for some biological structures. Polarisation, Matière et Rayonnement, Société Française de Physique Edition. P.U.F., Paris, France.
4. Ford, L. H. 2003. Estimate of the vibrational frequencies of spherical virus particles. *Phys. Rev. E.* 67:051924.
5. Saviot, L., D. B. Murray, A. Mermet, and E. Duval. 2004. Comment on estimate of the vibrational frequencies of spherical virus particles. *Phys. Rev. E.* 69:023901–1.
6. Fonoberov, V. A., and A. A. Balandin. 2004. Low-frequency vibrational modes of viruses used for nanoelectronic self-assemblies. *Phys. Status Sol. B.* 241:R67–R69.
7. Balandin, A. A., and V. A. Fonoberov. 2005. Vibrational modes of nano-template viruses. *J. Biomed. Nanotechnol.* 1:90–95.
8. Talati, M., and P. K. Jha. 2006. Acoustic phonon quantization and low-frequency Raman spectra of spherical viruses. *Phys. Rev. E.* 73: 011901–011906.
9. Tama, F., and C. L. Brooks III. 2002. The mechanism and pathway of pH induced swelling in cowpea chlorotic mottle virus. *J. Mol. Biol.* 318:733–747.
10. Tama, F., and C. L. Brooks III. 2005. Diversity and identity of mechanical properties of icosahedral viral capsids studied with elastic network normal mode analysis. *J. Mol. Biol.* 345:299–314.
11. Yoneda, S., T. Yoneda, Y. Kurihara, and H. Umeyama. 2001. Motion of an antiviral compound in a rhinovirus capsid under rotational symmetry boundary conditions. *J. Mol. Graph. Model.* 21:19–27.
12. Lidmar, J., L. Mirny, and D. R. Nelson. 2003. Virus shapes and buckling transitions in spherical shells. *Phys. Rev. E.* 68:051910.
13. Zandi, R., D. Reguera, R. F. Bruinsma, W. M. Gelbart, and J. Rudnick. 2004. Origin of icosahedral symmetry in viruses. *Proc. Natl. Acad. Sci. USA.* 101:15556–15560.
14. Larson, S. B., S. Koszelak, J. Day, A. Greenwood, J. A. Dodds, and A. McPherson. 1993. Three-dimensional structure of satellite tobacco mosaic virus at 2.9 Å resolution. *J. Mol. Biol.* 231:375–391.
15. Larson, S. B., J. Day, A. Greenwood, and A. McPherson. 1998. Refined structure of satellite tobacco mosaic virus at 1.8 Å resolution. *J. Mol. Biol.* 277:37–59.
16. Freddolino, P., A. Arkhipov, S. Larson, A. McPherson, and K. Schulten. 2006. Molecular dynamics simulations of the complete satellite tobacco mosaic virus. *Structure.* 14:437.
17. Kuznetsov, Y. G., A. J. Malkin, R. W. Lucas, M. Plomp, and A. McPherson. 2001. Imaging of viruses by atomic force microscopy. *J. Gen. Virol.* 82:2025–2034.
18. Lindsay, S. M., M. W. Anderson, and J. R. Sandercock. 1981. Construction and alignment of a high performance multipass Vernier tandem Fabry-Perot interferometer. *Rev. Sci. Instrum.* 52:1478–1486.
19. Liu, J., L. Ye, D. A. Weitz, and P. Sheng. 1990. Novel acoustic excitations in suspensions of hard-sphere colloids. *Phys. Rev. Lett.* 65: 2602.
20. Penciu, R. S., M. Kafesaki, G. Fytas, E. N. Economou, A. Steffen, W. Hollingsworth, and W. B. Russel. 2002. Phonons in colloidal crystals. *Europhys. Lett.* 58:699–704.
21. Kuok, M. H., H. S. Lim, S. C. Ng, N. N. Liu, and Z. K. Wang. 2003. Brillouin study of the quantization of acoustic modes in nanospheres. *Phys. Rev. Lett.* 90:255502.
22. Speziale, S., F. Jiang, C. L. Caylor, S. Kriminski, C.-S. Zha, R. E. Thorne, and T. S. Duffy. 2003. Sound velocity and elasticity of tetragonal lysozyme crystals by Brillouin spectroscopy. *Biophys. J.* 85:3202–3213.

23. Tachibana, M., K. Kojima, R. Ikuyama, Y. Kobayashi, and M. Ataka. 2000. Sound velocity and dynamic elastic constants of lysozyme single crystals. *Chem. Phys. Lett.* 332:259–264.

24. Lee, S. A., M. R. Flowers, W. F. Oliver, A. Rupprecht, and S. M. Lindsay. 1993. Brillouin-scattering study of hyaluronic acid: dynamic coupling with the water of hydration and phase transitions. *Phys. Rev. E.* 47:677–683.

25. Ivanovska, I. L., P. J. de Pablo, B. Ibarra, G. Sgalari, F. C. MacKintosh, J. L. Carrascosa, C. F. Schmidt, and G. J. L. Wuite. 2004. Bacteriophage capsids: tough nanoshells with complex elastic properties. *Proc. Natl. Acad. Sci. USA.* 101:7600–7605.

26. Tachibana, M., H. Koizumi, and K. Kojima. 2004. Effect of intracrystalline water on longitudinal sound velocity in tetragonal hen-egg-white lysozyme crystals. *Phys. Rev. E.* 69:051921–051925.

27. Dujardin, E., C. Peet, G. Stubbs, J. Culver, and S. Mann. 2003. Organization of metallic nanoparticles using tobacco mosaic virus templates. *Nano Lett.* 3:413–417.

28. Strable, E., J. Johnson, and M. Finn. 2004. Natural nanochemical building blocks: icosahedral virus particles organized by attached oligonucleotides. *Nano Lett.* 4:1385–1389.

29. Liu, W. L., K. Alim, A. A. Balandin, D. M. Mathews, and J. A. Dodds. 2005. Assembly and characterization of hybrid virus-inorganic nanotubes. *Appl. Phys. Lett.* 86:253108–3.

30. Duval, E., A. Boukenter, and B. Champagnon. 1986. Vibration eigenmodes and size of microcrystallites in glass: observation by very-low-frequency Raman scattering. *Phys. Rev. Lett.* 56:2052–2055.

31. Duval, E. 1992. Far-infrared and Raman vibrational transitions of a solid sphere: selection rules. *Phys. Rev. B.* 46:5795–5797.

32. Courty, A., A. Mermet, P. A. Albouy, E. Duval, and M. P. Pileni. 2005. Vibrational coherence of self-organized silver nanocrystals in F.C.C. supra-crystals. *Nat. Mater.* 4:395–398.

33. Saviot, L., and D. B. Murray. 2005. Longitudinal versus transverse spheroidal vibrational modes of an elastic sphere. *Phys. Rev. B.* 72: 205433–205436.

34. Murray, D. B., and L. Saviot. 2004. Phonons in an inhomogeneous continuum: vibrations of an embedded nanoparticle. *Phys. Rev. B.* 69:094305–094309.

35. Saviot, L., D. B. Murray, and M. d. C. Marco de Lucas. 2004. Vibrations of free and embedded anisotropic elastic spheres: application to low-frequency Raman scattering of silicon nanoparticles in silica. *Phys. Rev. B.* 69:113402–4.

36. Palpant, B., H. Portales, L. Saviot, J. Lermé, B. Prével, M. Pellarin, E. Duval, A. Perez, and M. Broyer. 1999. Quadrupolar vibrational mode of silver clusters from plasmon-assisted Raman scattering. *Phys. Rev. B.* 60:17107–17111.

37. Painter, P. C., L. E. Mosher, and C. Rhoads. 1982. Low-frequency modes in the Raman spectra of proteins. *Biopolymers.* 21:1469–1472.

38. Diehl, M., W. Doster, W. Petry, and H. Schober. 1997. Water-coupled low-frequency modes of myoglobin and lysozyme observed by inelastic neutron scattering. *Biophys. J.* 73:2726–2732.